Interference and Diffraction of Light

Adams, Jake
jake.adams@mail.utoronto.ca
1003847377

Jiang, Hansen
hansen.jiang@mail.utoronto.ca
1003192403

November 1 2018

Abstract

The purpose of this experiment was to analyze light intensity versus distance for a laser diffraction pattern to confirm the Heisenberg's Uncertainty Principle. Specifically, it is of important note how confirmation of the uncertainty principle in the lab can extend far beyond, and lead to an interpretation more broadly characteristic of all objects in the universe. In conclusion, the experiment demonstrated the distinct behaviors of both particle interference and diffraction and how these behaviors can be used to verify the Heisenberg's uncertainty principle.

Introduction

When light passes through a narrow slit, a distinct behavior occurs; with a screen placed a distance from the opposite side, a pattern of bright and dark bands can be observed. If a light sensor with a horizontal shift is placed in the position of the screen, the pattern can be scanned over and analyzed for similarities and differences between interference and diffraction. In this experiment, light intensity is used to confirm the Heisenberg's Uncertainty Principle.

Methods and Materials

- optics bench
- single slit disk
- multiple (double) slit disk
- rotary motion sensor
- aperture bracket
- linear translator
- low rpm driving motor
- Data Acquisition Device (DAQ)
- diode laser
- light sensor
- slit holder
- Interference and Diffraction program

Experimental Procedure

The single slit set was attached to the optics bench at 80cm, and the laser diode at 90cm. The rotary motion sensor, driving motor, aperture bracket, linear translator, and light sensor were mounted at the opposite end of the bench, with the aperture bracket positioned at 9.2cm and set on slit #6 and the light sensor gain set to 10x. The laser was then turned on and adjusted until the beam was central on the 0.16mm slit. A piece of paper was placed in front of the aperture screen and the diffraction pattern was observed. Next, the single slit set was replaced with the double slit disk and for each of the four combination slits, a diagram of the slit combination and its diffraction pattern were photographically recorded.

After familiarizing with the patterns, the double slit disk was swapped out with the single slit disk, with the 0.04mm slit positioned at the central point of the laser. The low rpm driving motor was switched on momentarily to position the light sensor to one side of the diffraction pattern. Then, the room lights were put out and the Interference and Diffraction program was initialized to prepare for data acquisition. Once

ready, the program began recording as the motor (switched on SLOW mode) moved the light sensor across the laser pattern until it reached the opposite end of the pattern, a distance of approximately 14cm. It is of slight importance to note that there was an issue with our setup, in that the data could only be collected in one direction–when the sensor was moving to the right. Nevertheless, this did not have any affect on the data collection. The data was exported and saved, and then the process was repeated with the light sensor on slit #4. From the acquired data, the slit width's were calculated using the equation, $asin\theta = m'\lambda$. This procedure was then repeated using a slit width 0.08mm.

With this portion of the experiment completed, the double slit disk was then used in place of the single slit disk and set to slit separation 0.25mm and slit width 0.04mm. The light sensor remained on slit #4. Then, the same process was followed as for the single slit portion of the procedure, once with the light sensor gain set to 10x, another with it set to 100x, and once more set to 1x. This was repeated for two other double slits, specifically one set to slit separation 0.50mm and slit width 0.04mm, and the other set to slit separation 0.25mm and slit width 0.08mm, both recorded with the light sensor gain on 100x.

For the diffraction pattern analysis, the diffraction experiment was again set up with a slit width 0.16mm and a laser-to-sensor distance of approximately 104.9cm. The resulting laser pattern was recorded.

Results

For a single slit interference pattern, intensity as a function of position x from the zero-location of the motor, becomes

$$I_{single}(x) = I(0)\left(\frac{\sin\left(\frac{\pi a}{\lambda}\cdot\frac{x-o}{\sqrt{(x-o)^2+L^2}}\right)}{\frac{\pi a}{\lambda}\cdot\frac{x-o}{\sqrt{(x-o)^2+L^2}}}\right)^2 \tag{1}$$

where a is the slit width, o is the offset of the center of the pattern, i.e. the intensity function's highest peak, and L is the distance from the sensor aperture and the light diode aperture. For the single slit experiment, $L = 78.3 \pm 0.1$cm.

For a double slit diffraction pattern, the intensity is affected by the interference between the light from each slit, resulting in the equation for double slit pattern intensity,

$$I_{double}(x) = I(0)\ \cdot\cos^2\left(\frac{\pi d}{\lambda}\cdot\frac{x-o}{\sqrt{(x-o)^2+L^2}}\right)\cdot\left(\frac{\sin\left(\frac{\pi a}{\lambda}\cdot\frac{x-o}{\sqrt{(x-o)^2+L^2}}\right)}{\frac{\pi a}{\lambda}\cdot\frac{x-o}{\sqrt{(x-o)^2+L^2}}}\right)^2 \tag{2}$$

where d is the slit separation, a is the slit width of both slits, and all other variables are as in Equation 1. For the double slit experiment, the diode was moved to the end of the equipment so that $L = 104.9 \pm 0.1$cm.

Using Equations 1 and 2 as the model functions in `scipy.optimize.curve_fit()` along with the known variables $\lambda = 650$nm, $L_{single} = 0.783$m, and $L_{double} = 1.049$m, optimum fit parameter values can be found for the data sets to compare with the expected parameter values. These values, including the ratio $a : \lambda$, along with the plots they result in, can be seen in detail in Appendices A and B, respectively.

From Figure 13, the relative heights of secondary maxima $\frac{I(\theta_i)}{I(0)}$ can be calculated for the intensity I at angle θ_i to the normal, where $I(\theta_i)$ is the intensity of the ith secondary maximum.

i	$\frac{I(\theta_i)}{I(0)}$	θ_i (°)
1	0.0498	1.35
2	0.0194	2.24
3	0.0108	3.18
4	0.00209	4.03

Table 1: relative heights of secondary maxima, Figure 13

Discussion

Plots with notable goodness of fit values are as below.

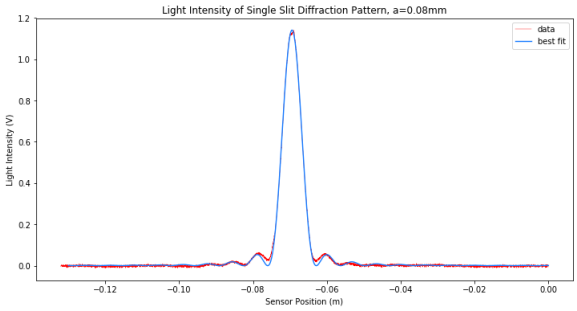

Figure 1: data and fit plot of single slit pattern

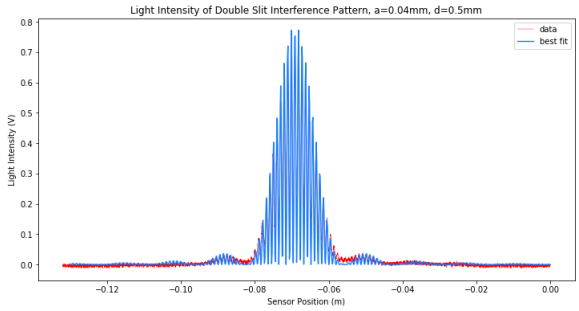

Figure 2: data and fit plot of double slit pattern

Figures 1 and 2 are the strongest fits between the collected data and the model function using the optimum parameters, as calculated by `curve_fit()`. Their goodness of fit is represented by $\chi^2_{red} = 0.7158$, and $\chi^2_{red} = 0.9196$, respectively. This is likely a result of using the appropriate gain setting at 100x, as the relative intensity maximum is around 1.0, along with the overall noise and uncertainty being relatively low. The result of inappropriate gain settings can be observed in the following plots of data.

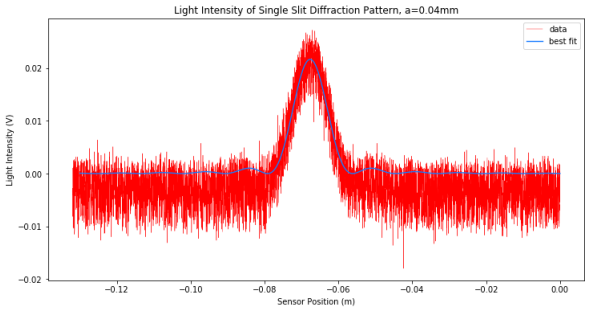

Figure 3: data and fit plot of single slit pattern

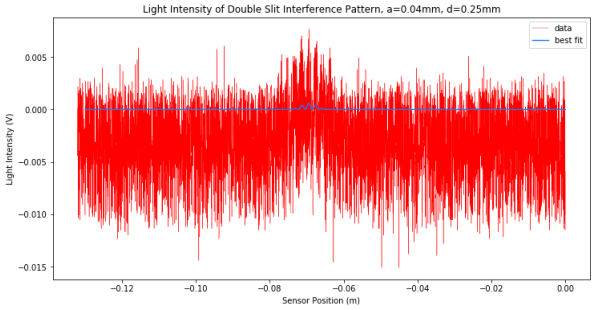

Figure 4: data and fit plot of double slit pattern

While `curve_fit()` attempts to optimize the parameters for the functions, it can only match with relativity to the noise of the data. Figure 3 demonstrates the inability to make sense out of inappropriately noisy data, especially computationally. Visually, the peak and shape of the function are similar to those of the other single slit patterns, but attempting to model the underlying function is difficult. Their goodness of fits are represented by $\chi^2_{red} = 0.2579$, and $\chi^2_{red} = 0.01400$, respectively. Since these values are $<< 1$, their corresponding model-parameter fits can be said to be over-fit: that is, the fit overestimates its accuracy to the data, which is wildly variant.

Heisenberg Uncertainty Verification

The data should be able to verify the Heisenberg Uncertainty Principle in the form

$$\frac{a}{\lambda}\sin\left(\tan^{-1}\frac{l}{b}\right) = 1 \tag{3}$$

where a is the slit width, λ is the wavelength of light, l is the half width of the central maximum of a single slit pattern, and b is the distance from the sensor aperture and the laser aperture. Using the data from the specified slit widths, the following is the result.

a(mm)	Equation 3 LHS	σ	% error	Figure #
0.04	0.9331	0.8	6.685	5
0.08	0.9895	2	1.047	6
0.16	1.197	3	19.75	7

Table 2: Equation 3 verification attempts

Since the results are within σ of the expected value of Equation 3 RHS = 1, then the data can be said to verify the Heisenberg Uncertainty Principle. However as the resulting uncertainties are relatively large, the results are not entirely conclusive. With more accurate measurements, the result is expected to be the same, with lower variances.

This discrepancy can be attributed to experimental sources of error. As can be noted in the data underneath the best fit plot for the double slit patterns, especially as in Figure 14, the central maximum pattern does not intercept with zero before spiking up again. This does not appear to be an issue of sampling time, as there are many points around where the zero-intercepts *should* be. As observed during the data collection of the double slit data, the closeness of the pattern allowed for the light from each slit to interfere imperfectly on the sensor screen. As a result, the base intensity was not zero, but rather a bump of underlying intensity. In addition, issues in angling the pattern to be perfectly horizontal with the sensor may have led to asymmetrical data, as with Figure 11. The high relative uncertainty can also be attributed to inappropriate noise levels as discussed above. A larger source of error depends on the accuracy of the data to the "actual" intensity function, and where the points for determining the half-width of the central maximum (l) are chosen to be. Despite these sources of error, the values are appropriately in range of the expected value of 1.

Questions

1. The light source remained the same for both single and double slit experiments. Specifically, the light's wavelength λ. This affects the horizontal scale of the intensity function for both patterns. As well, the horizontal offset was around the same area, since the horizontal position of the laser-lens-screen did not change, only the lens and the positions of the three. Thus, while the specific functions of the different patterns varied, the overall shape remained similar.

2. The distance from the central maximum to the first minimum for the single slit pattern was on average less than the distance from the central maximum to the first diffraction minimum in the double slit pattern.

3. The destructive interference of the light emerging from the two slits causes dark bands on the interference pattern, i.e. where the amplitude of the peaks goes to zero. The slit separation distance determines where this behavior occurs. As discussed, sources of error led to the observed pattern never having precise "zeros"- that is, some light always interfered to form a base intensity $I_{base} > 0$.

4. In theory, there should be 15 maximas in the envelope.

5. In practice, there are 13. An argument could be made for 15, though the bumps become difficult to distinguish from noise when relatively close to zero intensity.

Conclusion

Through observation and analysis of the laser patterns produced by light diffracting through different slits, the Heisenberg's uncertainty principle is affirmed.

Appendix

A Data Tables

a(mm)	a_{fit} (mm)	σ_a ($\pm 10^{-5}$mm)	$\frac{a_{fit}}{\lambda}$	Figure#
0.04	0.04	4	60.3 ± 0.06	5
0.08	0.08	4	119 ± 0.07	6
0.04	0.04	60	67.9 ± 0.9	7
0.16	0.12	9	186 ± 0.1	8
0.04	0.04	2	62.0 ± 0.2	9

Table 3: single slit optimum fit data

I_{fit} (V)	σ_I ($\pm 10^{-4}$V)	o_{fit} (cm)	σ_o ($\pm 10^{-4}$cm)	χ^2_{red}	Figure#
0.264	2	6.95	6	0.2505	5
1.13	6	6.94	2	0.7158	6
0.0216	3	6.77	60	0.2579	7
3.92	30	7.59	1	10.69	8
0.0643	3	6.80	20	0.2512	9

Table 4: single slit optimum fit data, continued

a(mm)	a_{fit} (mm)	d(mm)	d_{fit}(mm)	$\frac{a_{fit}}{\lambda}$	Figure #
0.04	$0.09 \pm 1 \cdot 10^{-1}$	0.25	$0.26 \pm 9 \cdot 10^{-2}$	140 ± 168	10
0.04	$0.03 \pm 2 \cdot 10^{-4}$	0.25	$0.25 \pm 1 \cdot 10^{-4}$	52.1 ± 0.3	11
0.04	$0.03 \pm 1 \cdot 10^{-4}$	0.25	$0.25 \pm 9 \cdot 10^{-5}$	53.6 ± 0.2	12
0.04	$0.04 \pm 2 \cdot 10^{-4}$	0.50	$0.50 \pm 1 \cdot 10^{-4}$	56.4 ± 0.003	13
0.08	$0.07 \pm 2 \cdot 10^{-4}$	0.25	$0.25 \pm 1 \cdot 10^{-4}$	113 ± 0.2	14

Table 5: double slit optimum fit data

I_{fit} (V)	σ_I ($\pm 10^{-3}$V)	o_{fit} (cm)	σ_o ($\pm 10^{-4}$cm)	χ^2_{red}	Figure #
0.000584	0.7	6.95	500	0.01400	10
0.187	0.9	6.76	2	0.06712	11
0.674	2	6.94	1	0.3072	12
0.786	4	6.92	1	0.9196	13
3.44	7	6.93	1	1.748	14

Table 6: double slit optimum fit data, continued

B Plots

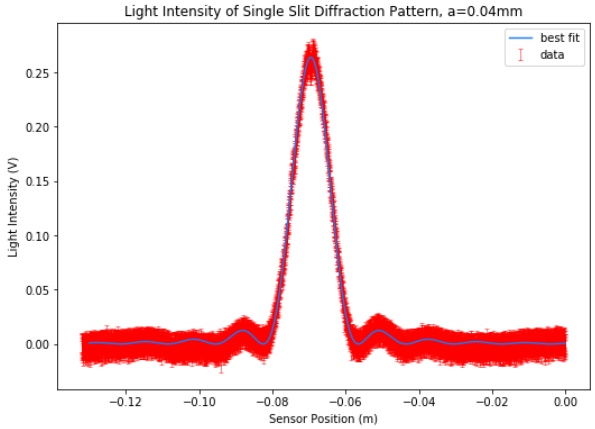

Figure 5: error bar and fit plot of single slit pattern

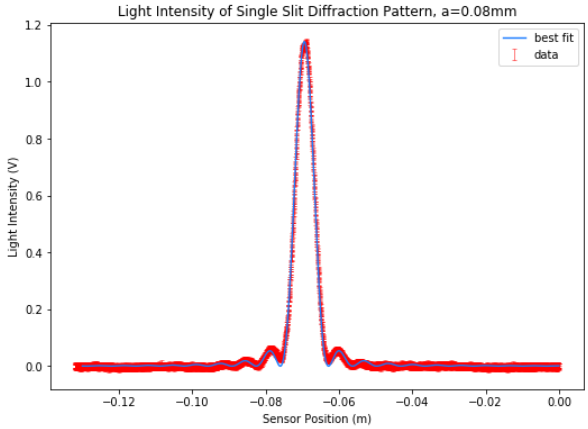

Figure 6: error bar and fit plot of single slit pattern

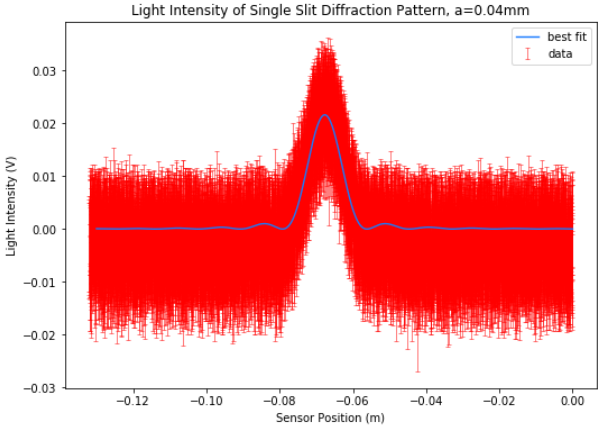

Figure 7: error bar and fit plot of single slit pattern

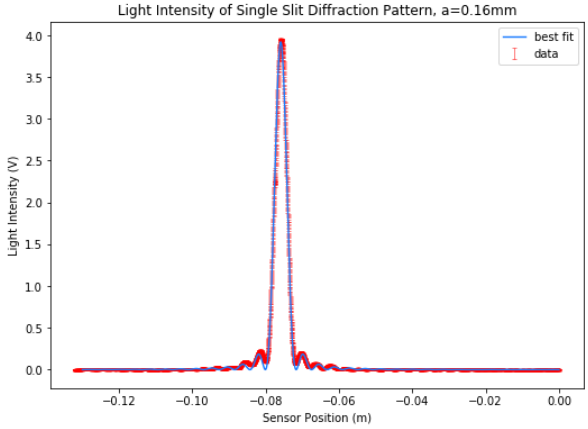

Figure 8: error bar and fit plot of single slit pattern

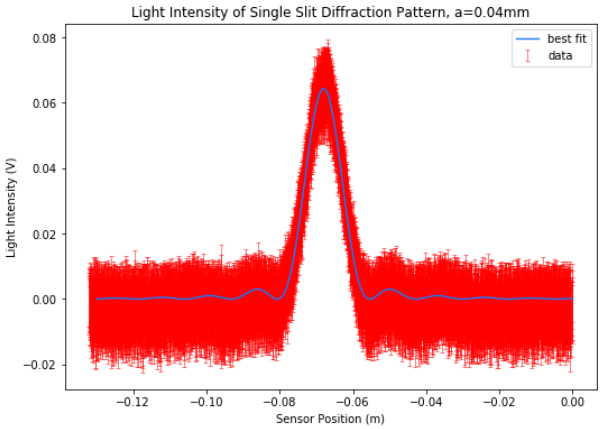

Figure 9: error bar and fit plot of single slit pattern

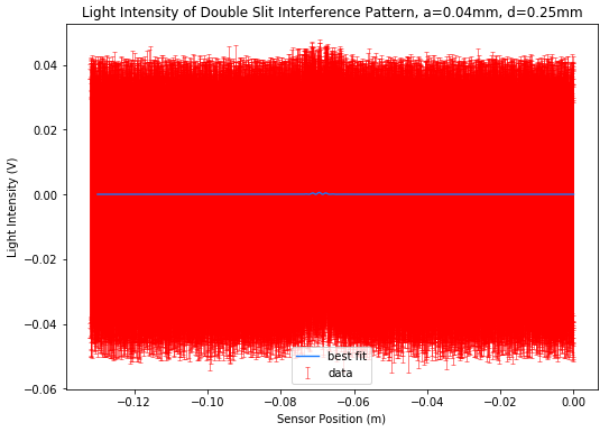

Figure 10: error bar and fit plot of double slit pattern

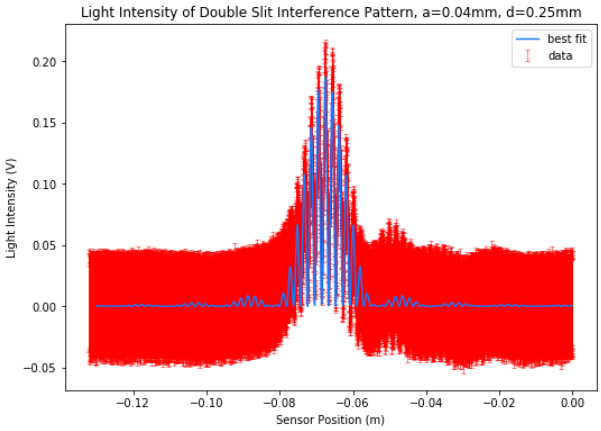

Figure 11: error bar and fit plot of double slit pattern

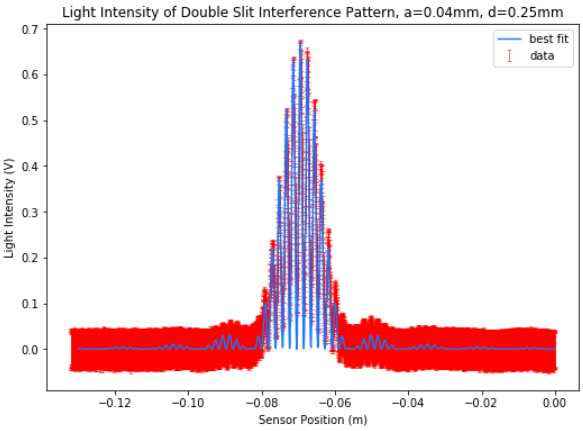

Figure 12: error bar and fit plot of double slit pattern

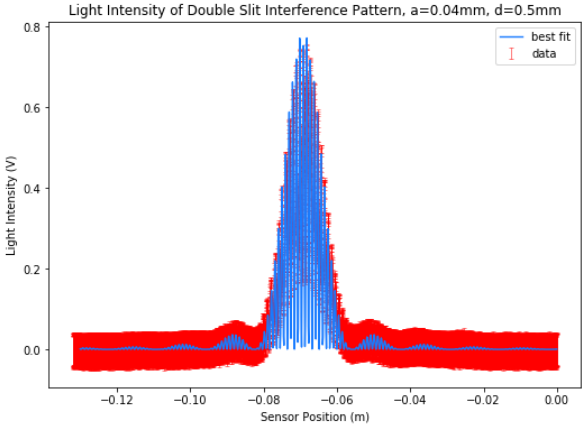

Figure 13: error bar and fit plot of double slit pattern

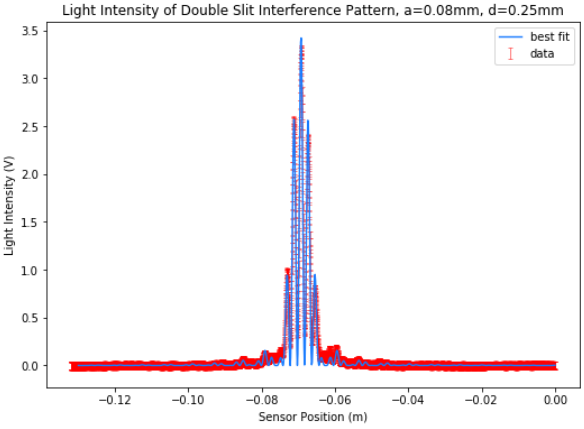

Figure 14: error bar and fit plot of double slit pattern